Discovery of a New Stellar Subpopulation Residing in the (Inner) Stellar Halo of the Milky Way

José G. Fernández-Trincado[1,2,11], Timothy C. Beers[3], Vinicius M. Placco[3], Edmundo Moreno[4], Alan Alves-Brito[5], Dante Minniti[6,7,8], Baitian Tang[9], Angeles Pérez-Villegas[10], Céline Reylé[2], Annie C. Robin[2], and Sandro Villanova[11]

[1] Instituto de Astronomía y Ciencias Planetarias, Universidad de Atacama, Copayapu 485, Copiapó, Chile; jose.fernandez@uda.cl, jfernandezt87@gmail.com
[2] Institut Utinam, CNRS-UMR 6213, Université Bourgogne-Franche-Comté, OSU THETA Franche-Comté, Observatoire de Besançon, BP 1615, F-251010 Besançon Cedex, France; jfernandez@obs-besancon.fr
[3] Department of Physics and JINA Center for the Evolution of the Elements, University of Notre Dame, Notre Dame, IN 46556, USA
[4] Instituto de Astronomía, Universidad Nacional Autónoma de México, Apdo. Postal 70264, México D.F., 04510, México
[5] Universidade Federal do Rio Grande do Sul, Instituto de Física, Av. Bento Gonçalves 9500, Porto Alegre, RS, Brazil
[6] Depto. de Cs. Físicas, Facultad de Ciencias Exactas, Universidad Andrés Bello, Av. Fernández Concha 700, Las Condes, Santiago, Chile
[7] Millennium Institute of Astrophysics, Av. Vicuna Mackenna 4860, 782-0436, Santiago, Chile
[8] Vatican Observatory, V-00120 Vatican City State, Italy
[9] School of Physics and Astronomy, Sun Yat-sen University, Zhuhai 519082, People's Republic of China
[10] Universidade de São Paulo, IAG, Rua do Matão 1226, Cidade Universitária, São Paulo 05508-900, Brazil
[11] Departamento de Astronomía, Casilla 160-C, Universidad de Concepción, Concepción, Chile

Abstract

We report the discovery of a unique collection of metal-poor giant stars that exhibit anomalously high levels of ^{28}Si, clearly above typical Galactic levels. Our sample spans a narrow range of metallicities, peaking at -1.07 ± 0.06, and exhibits abundance ratios of [Si, Al/Fe] that are as extreme as those observed in Galactic globular clusters (GCs), and Mg is slightly less overabundant. In almost all the sources we used, the elemental abundances were redetermined from high-resolution spectra, which were reanalyzed assuming LTE. Thus, we compiled the main element families, namely, the light elements (C, N), α-elements (O, Mg, Si), iron-peak element (Fe), s-process elements (Ce, Nd), and the light odd-Z element (Al). We also provide dynamical evidence that most of these stars lie on tight (inner) halo-like and retrograde orbits passing through the bulge. Such kinds of objects have been found in present-day halo GCs, providing the clearest chemical signature of past accretion events in the (inner) stellar halo of the galaxy, possibly formed as the result of dissolved halo GCs. Their chemical composition is, in general, similar to that of typical GC populations, although several differences exist.

1. Introduction

The existence of chemical anomalies in field stars has been known for a long time, especially in the form of nonevolved or scarcely evolved stars on the main sequence and evolved red giant branch stars. While there is support in the literature that a small fraction, ~1%–13%, of the present-day population of the stellar halo (Martell et al. 2016; Koch et al. 2019) of the Milky Way is filled with a unique collection of stars that are extremely common in clusters and also characterized by distinctive chemical anomalies in a number of light elements, namely, Al, N, Na, and K with respect to Fe, and well above typical Galactic levels at a range of metallicities, to date a unifying explanation of the processes acting to produce such high levels of abundance anomalies or nucleosynthetic pathways in field stars remains elusive (Fernández-Trincado et al. 2016, 2019a, 2019b; Pereira et al. 2019). Hence, the more common assumption is that the majority of such unexplained objects that reside in the field that replicate or exceed the extreme abundance patterns seen in globular clusters (GCs) are commonly referred to as tidally dissipated remnants of GCs (unless they are part of a binary system), as they have similar properties to that of the present-day GCs (Fernández-Trincado et al. 2016, 2017, 2019a, 2019c; Martell et al. 2016; Schiavon et al. 2017; Koch et al. 2019, among others), with only a

handful of exceptions that are often associated with other stellar associations like dwarf galaxies (e.g., Hasselquist et al. 2019).

Among the variety of objects with an exotic chemical composition that populate Galactic GCs, stars with anomalously high levels of [Si/Fe] ratios ($\gtrsim +0.6$, which we henceforth refer to as silicon-rich stars) among metal-poor stars are surely among those still presenting many riddles to astronomers. The Si overabundance of GC stars that can be produced, under some assumptions, i.e., the Mg–Si anticorrelation found in several GCs (Carretta & Bragaglia 2019) is of particular importance because it pinpoints the "leakage" mechanism from Mg–Al cycle on ^{28}Si as the major source of the phenomenon, i.e., when the ^{27}Al(p, γ)^{28}Si reaction takes over ^{27}Al(p, α)^{24}Mg a certain amount of ^{28}Si is produced by p-captures (Karakas & Lattanzio 2003). However, temperatures in excess of >100 MK are required to activate the relevant reactions attained in the polluters, which thus provide the overproduction of [Si/Fe] ratios (see, e.g., Arnould et al. 1999), and apparently are possible only among stars in a subset of GC stars (Masseron et al. 2019). These silicon-rich stars apparently tend to form at all metallicities (Carretta & Bragaglia 2019), so it is probable that the polluting source is extant at all metallicities.

Thus, the task to identify such kinds of stars beyond GC environments may reveal any chemical peculiarity and also
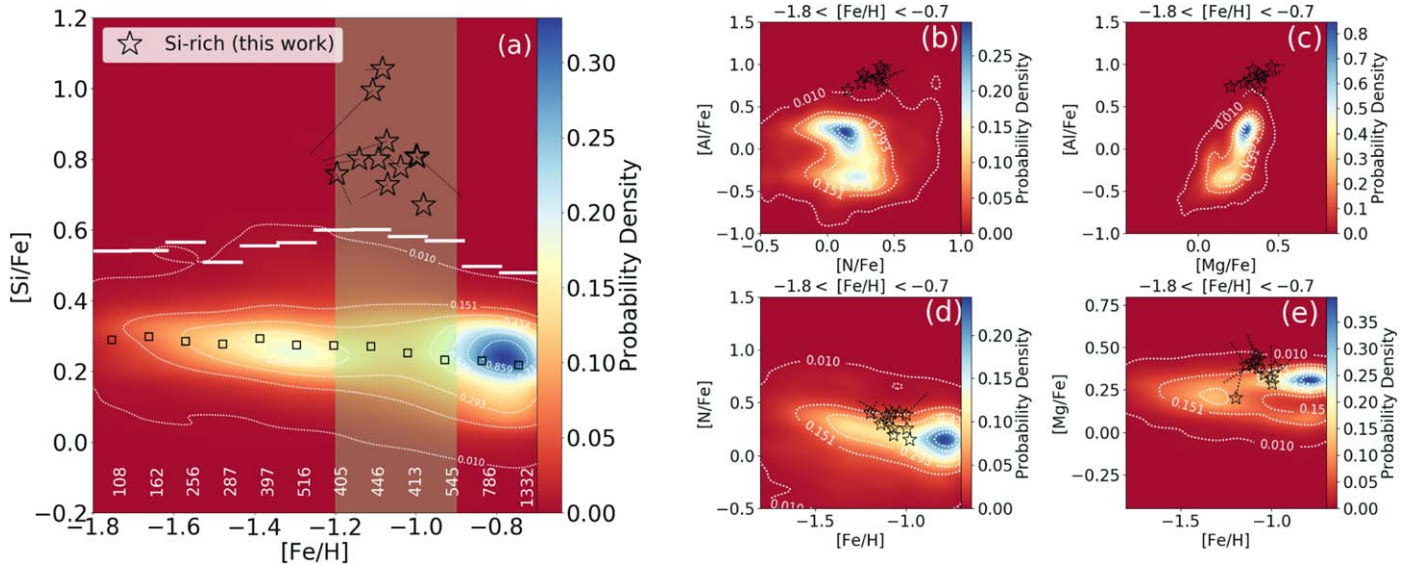
Figure 1. Kernel density estimation (KDE) of data displayed as a density colormap (panels (a), (b), (c), (d), and (e)), with a set of density contours as white dotted lines, while the color indicates the probability density. The black open star symbols refers to the abundance ratios ([X/Fe]$_{\rm spe}$) of the silicon-rich stars, while the black dotted line shows the [X/Fe]$_{\rm pho}$ abundance ratios (see Table 2). In panel (a) a shaded vertical area highlights the metallicity range ($-1.2 <$ [Fe/H] < -0.9 dex) in which stars exhibit dramatic enhancement in silicon abundance, while the number of stars of each bin in the main body are shown at the center of the bin at the middle bottom panel, and the black open squares show the mean value of [Si/Fe] by bin, and the white line-segment indicates the selection criteria where [Si/Fe] $> \langle$[Si/Fe]$\rangle + 3\sigma_{\rm [Si/Fe]}$. The error bars are estimates of the uncertainties ($\sigma_{\rm total} = \sqrt{\sigma^2_{\rm [X/H],T_{\rm eff}} + \sigma^2_{\rm [X/H],\log g} + \sigma^2_{\rm [X/H],\xi_t} + \sigma^2_{\rm mean}}$) computed in the same way as Fernández-Trincado et al. (2019a).

allow us to constraint the search for stellar tidal debris of defunct GCs in the (inner) stellar halo of the Milky Way, implying that ^{28}Si would be an important chemical species for a genetic link to GCs stars, thus playing a role in determining whether light element anomalies arise from nuclear processing within evolved stars born within GCs environments or are tied to a certain epoch in the Milky Way's evolution. It is also in line with previous suggestions that the (inner) stellar halo may have formed a nonnegligible fraction of its mass ex situ, according to which these stars originate from the dissolution of a population of accreted GCs (Martell et al. 2016).

So far, stars with significantly enhanced aluminum paired with silicon enrichment have thus far only been identified in a few GC environments (Masseron et al. 2019). The origin of such signs remain unknown, as does the reason for its apparent exclusivity to GCs environments. In this Letter we report on the serendipitous discovery by the Apache Point Observatory Galactic Evolution Experiment (APOGEE-2; Majewski et al. 2017) of a unique collection of mildly metal-poor, field giant stars, which exhibit silicon overabundances ([Si/Fe] $\gtrsim +0.6$) significantly higher than typical Galactic abundances of [Si/Fe] $< +0.5$, which we hypothesized that all silicon-rich stars were formed in GC environments and were later lost to the field when the stellar clusters were ultimately disrupted and that also contributed to the (inner) stellar halo buildup.

2. Discovery of a New Stellar Subpopulation

We report the discovery of an unexpected and exceptional enhancement of [Si/Fe] abundance ratios among mildly metal-poor giant stars ([Fe/H] < -0.7) in the Galactic field, which have been identified from the $\sim$270,000 APOGEE-2 giant stars (14th data release of SDSS; Abolfathi et al. 2018), that exhibit significantly enhanced [Si/Fe] and [Al/Fe] abundance ratios. Since we are primarily interested in abundance anomalies of metal-poor stars, our focus in this work is on giant stars with

metallicities [Fe/H] < -0.7.[12] We selected a sample of giant stars, adopting conservative cuts on the columns of the APOGEE-2 catalog in the following way: (i) signal-to-noise ratio (S/N) > 70 pixel^{-1}; (ii) 3500 K $< T_{\rm eff} < 6000$ K; (iii) log $g < 3.6$; and (iv) ASPCAPFLAG[13] $= 0$. Following the conventions in the literature (see, e.g., Schiavon et al. 2017), we require nonenhanced carbon stars with [C/Fe] $< +0.15$, because such stars are commonly found in GCs, and the surface abundance of stars enhanced in carbon ([C/Fe] $> +0.15$) may have been modified by mass transfer from aysmptotic giant branch (AGB) companions (e.g., Lucatello et al. 2006). The final sample selected amounts to a total of 5653 stars. The method in deriving atmospheric parameters and abundances is identical to that of Fernández-Trincado et al. (2019a), adopting the Brussels Automatic Stellar Parameter (BACCHUS) code (Masseron et al. 2016). The results are listed in Table 2.

A new stellar subpopulation was identified for searching for outliers in the [Si/Fe]–[Fe/H] abundance plane. We determined the boundary between these outliers and the Milky Way stars by identifying the trough in the [Si/Fe] distribution over 12 metallicity bins and performing a single Gaussian component fit. We label all stars with [Si/Fe] abundance more than $3\sigma_{\rm [Si/Fe]}$ above the median [Si/Fe] abundance value of the corresponding iron bin as "silicon-rich" (see Figure 1). The bins were chosen to ensure that at least $\sim$100 stars were in each bin. This returns 36 stars that appear silicon-rich relative to the full data set. We then eliminate three known GC stars from our sample, leaving 33 silicon-rich candidates.

---

[12] By requiring metallicity more metal-poor than -0.7 we minimize the presence of giants in the thin and thick disk, and by imposing a lower limit on metallicity of -1.8, allow for the inclusion of stars with reliable carbon and nitrogen abundances (see Fernández-Trincado et al. 2019a and references therein).

[13] This cut ensure that there were no major flagged issues, i.e., low-S/N, poor synthetic spectral fit, stellar parameters near grid boundaries, among others.
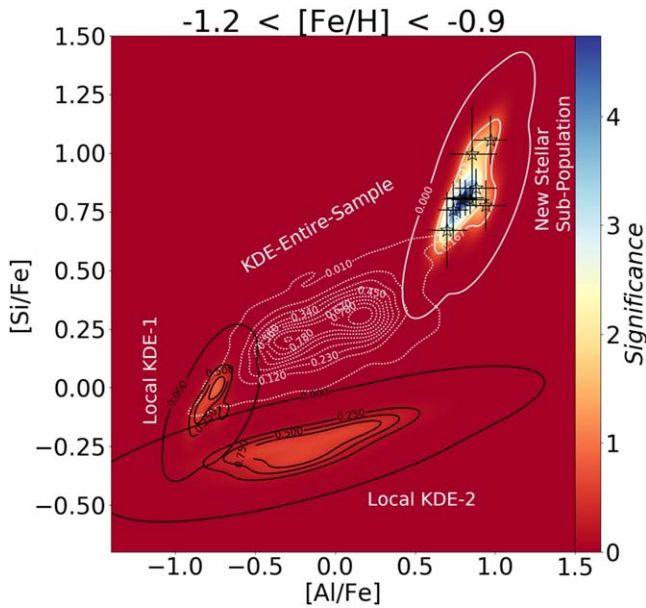
Figure 2. Kernel density estimation (KDE) models in the [Si, Al/Fe] plane for the entire sample (white dashed–dotted contour) in the metallicity range $-1.2 <$ [Fe/H] < -0.9 compared to the KDE models of two arbitrary local volumes that contain some data points (black solid contours), and the KDE of the new stellar subpopulation (white line contour). The color indicates the significance of each local volume as compared to the background level.

In order to confidently state chemical tagging results for this data set, we also require enhanced aluminum ([Al/Fe] $\gtrsim +0.5$), as a lower aluminum abundance is not by itself a sufficient indicator of a GC-like abundance pattern in the Galactic field. If high levels of Al enrichments are found, this would imply that such Si–Al-rich giant field stars and second-generation GC stars could potentially be the same kind of stellar objects, with similar nucleosynthetic histories. This leaves us with 11 likely Si–Al-rich red-giants with high-quality spectra and reliable parameters and abundances. Note that for the newly identified silicon-rich stars, there are no nearby GCs showing direct association, based on the chemical/dynamical properties. To further assess the statistical significance of the newly identified stellar subpopulation, we ran a kernel density estimation (KDE) over this sample, and compared it with the tail of the main Milky Way locus (silicon-normal stars), i.e., with some arbitrary local volume that contains some data points as illustrated in Figure 2. Finally, in Figure 2, we plot the KDE models over our data to demonstrate that there is a true low-density valley separating the silicon-normal population from the silicon-rich population; it gives us an idea of the significance of our finding, which exceeds the background level by a factor of ~4, which is also significant as compared to the two arbitrary local volumes of the entire sample. A set of contour lines is set as a visual aid. From Figure 2, we can see how the local "silicon-rich" sample occupies a separate and significant locus of stars beyond [Si/Fe] $> +0.5$, which is not on the main bulk of the KDE of the entire sample.

A comparison is presented in Figure 3, where the spectra of a silicon-rich and a silicon-normal star are shown in the relevant wavelength range containing the Si I lines, indicated by vertical tick marks. The silicon-rich star has remarkably stronger Si I lines which, in view of the similarity between the two stars in all the other relevant parameters, can only mean that it has a much higher silicon abundance. Both ASPCAP (García Pérez et al. 2016) and our line-by-line manual analysis with BACCHUS tell us that [Si/Fe] in the silicon-rich star is higher than the silicon-normal star by $\sim 3.73\sigma$. In doing chemical tagging in the disk (thick), we have moved past just asking whether stars could have formed in GCs, and now we are looking for ways to understand several different types of chemically anomalous stars.

3. Results and Discussion

The Si overabundances reported here are significantly above the typical value measured in the Milky Way, and are strikingly similar those observed in Galactic GC environments.

3.1. Chemical Evidence for a New Stellar Subpopulation in the Inner Stellar Halo of the Milky Way

Figure 1 (top panel) suggests that a new subpopulation of stars chemically differentiated by their highest [Si/Fe] abundance ratios has been identified in the galaxy, clumped at values [Si/Fe] $\sim +0.82 \pm 0.11$ (which we henceforth refer to as silicon-rich stars), and clearly separated from the main body of silicon-normal stars for [Si/Fe] $< +0.5$. Regarding their metallicity distribution, the silicon-rich stars range between $-1.2 \lesssim$ [Fe/H] $\lesssim -0.9$, with a mean value of [Fe/H] $\pm \sigma_{[Fe/H]} = -1.07 \pm 0.06$, suggesting in fact a possible association with the thick disk or halo. If we make a simplistic assumption that Milky Way stars in that metallicity range can be modeled as a Gaussian with a mean of [Si/Fe] $=$ 0.26 and $\sigma_{[Si/Fe]} = 0.11$ (over 1458 stars in that iron bin), the probability of drawing a silicon-rich star ([Si/Fe] > 0.67) star at the same metallicity bin is $<0.1\%$ (3.73σ). The probability of drawing a star of that metallicity with [Si/Fe] > 0.6 from the galaxy population is small. As such, the following is devoted to exploring these object in more detail.

Figure 1(a) shows the trend of [Si/Fe] with metallicity for accreted halo stars, canonical halo stars, and thick disk stars with [Si/Fe] $< +0.6$ dex (silicon-normal stars), which appear to be very mixed according to Hawkins et al. (2015). Hence, the discovery of such silicon-rich stars suggests that ^{28}Si might follow different nucleosynthesis pathway(s) and reveals a well-defined dichotomy between field giants and other Galactic environments (like GC stars), and it is possible that such objects may represent a population for stars evaporated from GCs.

From Figures 1(e), (f) we also note that silicon-rich stars exhibit slightly enriched levels of N and Mg than most Milky Way stars at the same metallicities, at least as far as observed dispersion is concerned, i.e., $\sigma_N = 0.09$ dex and $\sigma_{Mg} = 0.07$ dex, respectively, indicating a distinct formation history. In addition, there are chemistry similarities in [Mg/Fe] and [N/Fe] ratios between the silicon-rich stars and the population of stars in the innermost regions of the Galactic halo. Thus, N and Mg affirm that the silicon-rich stars could be a subpopulation of the same population as the high-Mg halo population (see, e.g., Hayes et al. 2018).

We emphasize that the enhanced abundances of [Si/Fe] in these objects is not only caused by the natural [Si/Fe] variations observed for field stars. To our knowledge, the only Galactic environments that contains a sufficient fraction of stars with a sufficiently enrichment in [Si/Fe] paired by the modest enrichment in [Al/Fe] are Galactic GCs (Masseron et al. 2019)
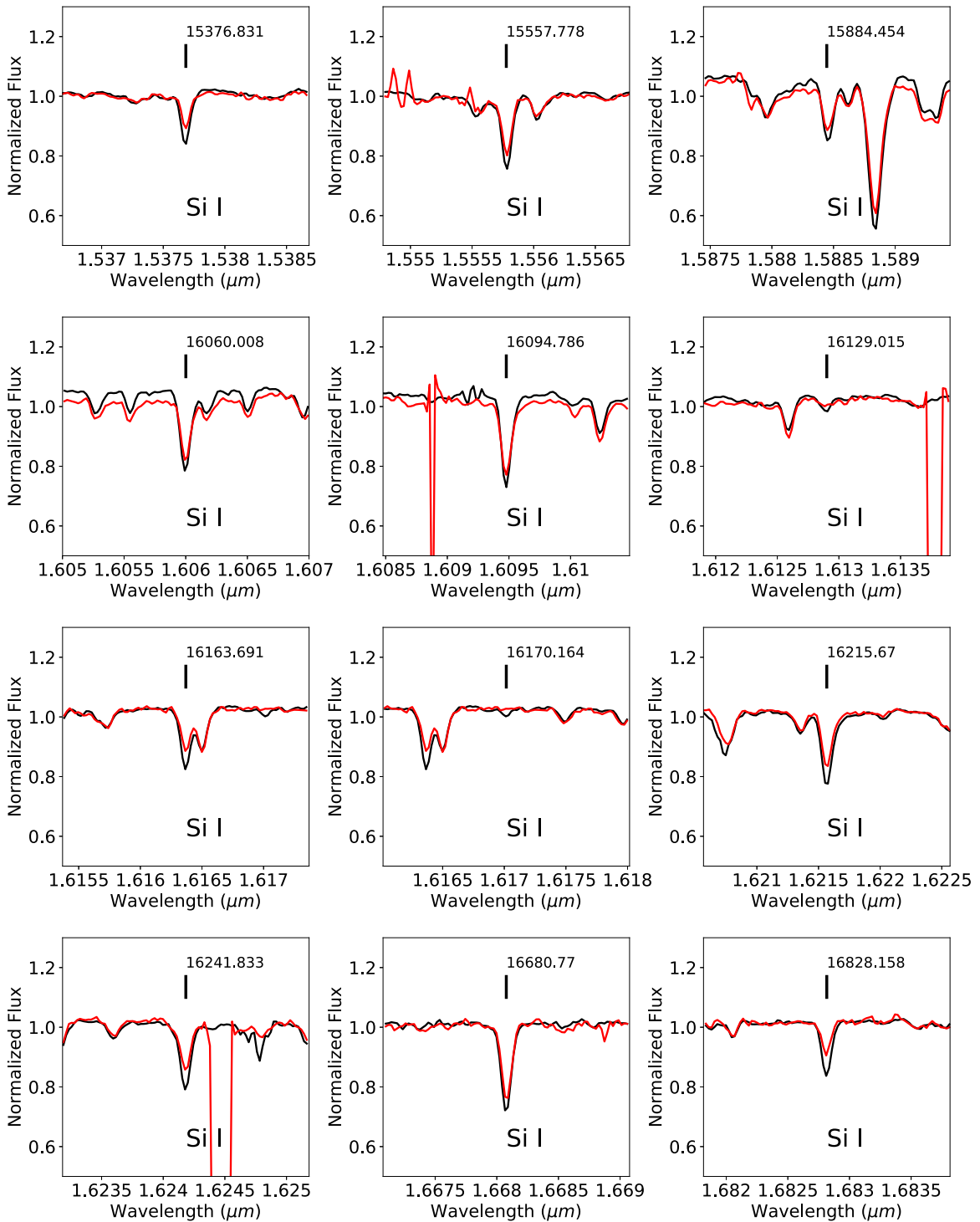
Figure 3. Comparison between the APOGEE-2 spectrum of a normal (red line, star: 2M14424814+4653219, $T_{\mathrm{eff}} = 4346$ K, $\log g = 1.66$, [Fe/H] $= -1.19$, [Si/Fe] $= +0.25$) and a silicon-rich giant star (black line, star: 2M19281906+4915086, $T_{\mathrm{eff}} = 4309$ K, $\log g = 1.71$, [Fe/H] $= -1.20$, [Si/Fe] $= +0.65$) around the Si I lines, with similar stellar parameters.

at similar metallicity. We conclude that it is difficult to explain high [Si/Fe] values of these sources with the typical history of silicon enrichment of the galaxy.

We computed the more probable Galactic orbit for 8/11 silicon-rich stars. For this, we combine precise proper motions from *Gaia* DR2 (Lindegren et al. 2018), radial velocity from APOGEE-2 (Nidever et al. 2015), and the inferred distances using StarHorse code (Queiroz et al. 2018), which

additionally include the cuts (SH_GAIAFLAG = "000" and SH_OUTFLAG = "00000") described in Anders et al. (2019), as input data in the new state-of-the-art orbital integration package GravPot16.[14] Table 1 lists the renormalized unit weight error (RUWE) and available distance for these sources

---

[14] https://gravpot.utinam.cnrs.fr

Table 1
Renormalized Unit Weight Error (RUWE) for 8 out of 11 Silicon-rich Stars Astrometrically Well Behaved, and Good Inferred Distances Using `StarHorse` (gdr2_contrib.starhorse)

APOGEE-2 ID	NgAl	chi2AL	Np	Gmag	BPmag	RPmag	RUWE	SH_GAIAFLAG	SH_OUTFLAG	$d_\odot$ (kpc) StarHorse	RV (km s^{-1}) APOGEE-2	$\mu_\alpha \cos(\delta)$ (mas yr^{-1}) Gaia DR2	μ_δ (mas yr^{-1}) Gaia DR2	Galactic Orbit GravPot16
2M13314691 +2804210	560	694.07	15	12.45	13.21	11.61	1.02	"000"	"00000"	6.14 ± 1.94	-1.72 ± 0.12	-7.32 ± 0.08	-6.54 ± 0.05	✓
2M15153684 +3501283	292	178.51	18	13.88	14.52	13.13	0.99	"000"	"00000"	11.0 ± 3.66	-308.45 ± 0.12	-4.14 ± 0.04	-7.74 ± 0.05	✓
2M16092248 +2449223	476	753.02	18	12.41	13.25	11.53	1.09	"000"	"00000"	6.34 ± 1.33	-92.29 ± 0.22	-9.28 ± 0.05	-1.51 ± 0.05	✓
2M16300791 +2537503	354	294.97	17	13.03	13.58	12.34	0.96	"000"	"00000"	4.89 ± 0.57	-255.29 ± 0.02	-3.02 ± 0.04	-9.39 ± 0.04	✓
2M16482145 −1930487	301	276.21	12	14.13	15.04	13.18	1.00	"000"	"00000"	7.88 ± 1.69	65.99 ± 0.03	-0.11 ± 0.07	-10.05 ± 0.05	✓
2M17155274 +2907368	279	203.76	17	13.77	14.44	12.99	1.09	"000"	"00000"	7.69 ± 1.48	-81.52 ± 0.03	-4.11 ± 0.04	-1.87 ± 0.05	✓
2M17214096 +4246147	185	194.90	16	12.83	13.48	12.07	0.91	"000"	"00000"	5.97 ± 1.40	-298.07 ± 0.05	-5.59 ± 0.05	-3.97 ± 0.06	✓
2M23341347 +4836321	400	313.58	18	13.88	14.75	12.97	0.98	"000"	"00000"	11.04 ± 3.01	-168.33 ± 0.15	2.28 ± 0.05	-0.43 ± 0.05	✓

Note. In this table, we consider only the subset of stars in the sample that respects the flags recommended in Anders et al. (2019), which corresponds to the most robust distances, i.e., SH_GAIAFLAG = "000" and SH_OUTFLAG = "00000" NgAl = astrometric_n_good_obs_al—chi2AL = astrometric_chi2_al—Np = VISIBILITY_PERIODS_USED—Gmag = phot_g_mean_mag—BPmag = phot_bp_mean_mag—RPmag = phot_rp_mean_mag. For each PM component we have accounted for the systematic uncertainty on the order of 0.035 mas yr^{-1} (Lindegren et al. 2018).
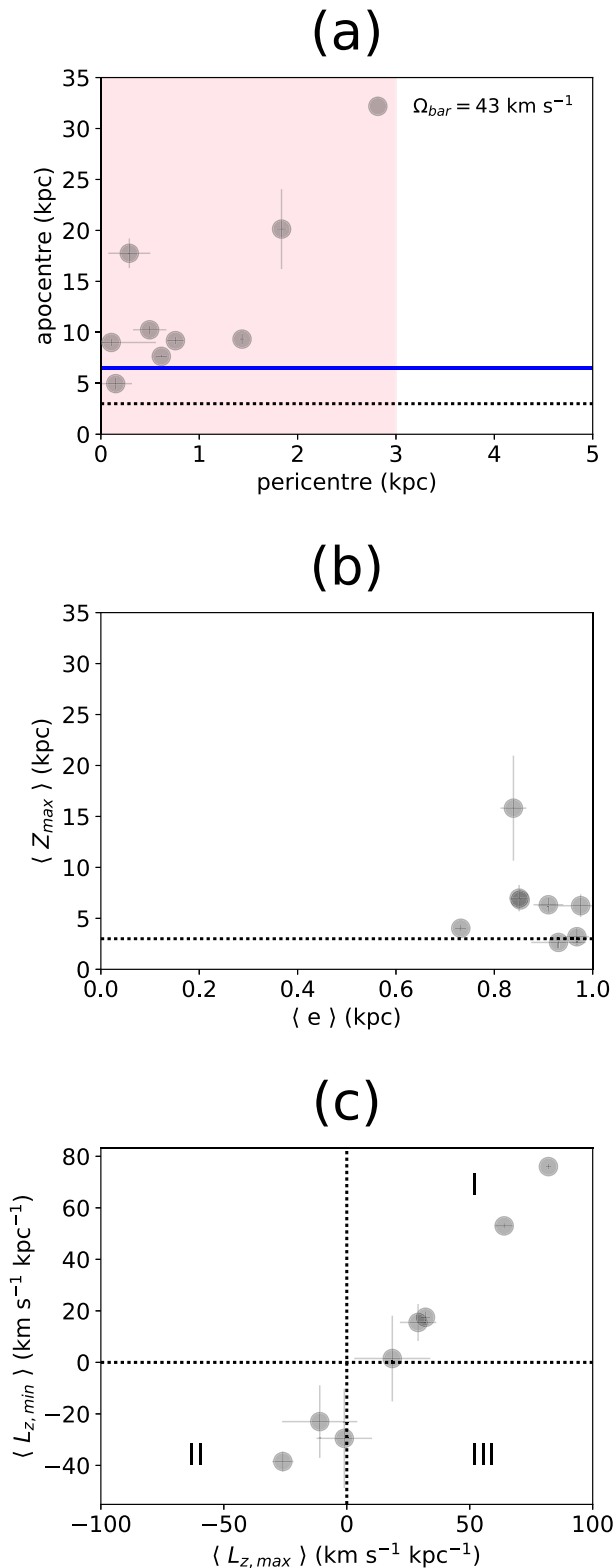
(a)

(b)

(c)

Figure 4. Orbital parameters of the silicon-rich stars. In panel (a), the shaded region and the black dotted line indicate the radius (3 kpc; Barbuy et al. 2018) of the Milky Way bulge, while the blue line indicates the location of the bar's corotation radius (CR ∼ 6.5 kpc); a star below the black dotted line would have a bulge-like orbit. In panel (b), the black dotted line represents the edge Z_{max} of the thick disk (∼3 kpc; Carollo et al. 2010). In panel (c), the black dotted lines divide the regions with prograde orbits (region II) with respect to the direction of the Galactic rotation, retrograde orbits (region I), and stars that have prograde–retrograde orbits at the same time (region III). The error bars show the uncertainty in the computed orbital parameters.

from the `gdr2_contrib.starhorse` table, where the typical RUWE is less than or equal to 1.4, indicating that these sources are astrometrically well behaved.

Since the true Galactic potential is not accurately known in the inner galaxy (<0.5 kpc), the results of our simulations may depend significantly on the assumed model in the inner galaxy, especially for those stars with orbital incursions closer to the Galactic center, assuming a $\Omega_{bar} = 43 \, \mathrm{km \, s^{-1}}$ (Bovy et al. 2019). The silicon-rich stars are found to have radial orbits, with pericenter values less than 2 kpc, apocenter values ranging between 4 and 20 kpc, eccentricities larger than 0.5, and a maximum vertical excursion from the Galactic plane ranging between 1.8 and 16 kpc. In Figure 4 and Table 2 we give some orbital parameters for each silicon-rich star; we refer the reader to Fernández-Trincado et al. (2019a) for details regarding all the parameters employed in our Galactic model. We find that these are not stars that live in the inner galaxy, and therefore those identified toward the bulge region are likely halo intruders in the Galactic bulge. Most of the silicon-rich stars exhibit retrograde orbits and have halo-like orbits, characterized by high eccentricities ($e > 0.5$). It is important to note that the large spread in the apocenter distance, in addition to stars having a prograde or a retrograde sense (see Figure 4(c)) with respect to the rotation of the bar, suggests that they cannot have a common origin (unless they were released from their parent at a very different time). In this sense, the predicted orbits would suggest that most of these stars were likely formed during the very early stages of the evolution of the Milky Way, in a similar way as Galactic GCs. These dynamical properties accompanied by the large enrichment in Si, as well as the modest enhancement in Al, and no evidence of an intrinsic Fe abundance spread (<0.06 dex), reveal that these objects were likely born from the same molecular cloud and later accreted during the initial phases of galaxy assembly and contributed to the old stellar populations of the inner stellar halo. In general, the evidence for a high [Si/Fe] peak might plausibly be explained by a previous accretion event in the Milky Way. However, the level of Al enhancement observed in this new subpopulation provides evidence that such stars are not from a dissolved dwarf galaxy (see, e.g., Hasselquist et al. 2019).

3.2. A GC Origin

We speculate that some of the silicon-rich stars found in the inner galaxy could be remnants of tidally disrupted infalling GCs. Figure 5 presents some light and s-process element patterns of the 11-star candidate pool identified by Si-enhanced stars compared with those obtained from a run of `BACCHUS` for GC stars (see, eg., Masseron et al. 2019) at a similar metallicity to our sample. Interestingly, similar silicon enhancements have been detected in Galactic GCs (Masseron et al. 2019). Also in these cases, abundances of elements other than silicon are similar to that observed for similar giant stars. Remarkably, most of the newly identified silicon-rich field stars exhibit light-/heavy-element abundances similar to typical Galactic GCs. It provides some clues for the uniqueness of the progenitor stars to GCs, and it is very likely that whatever process is responsible for such a level of [Si/Fe] enhancement observed in the Galactic field appears to be similar to whatever caused the unusual stellar populations in GCs. Similar to our silicon-rich stars, some Galactic GCs also exhibit interesting enrichment in s-process elements (e.g., Masseron et al. 2019) and anomalously high levels of aluminum, silicon, cerium, and

Table 2
Adopted Atmospheric Parameters of Our Target Stars, Frequency of Observation Per Object (N_{visits}), Signal-to-noise Ratio (S/N), Radial Velocity (RV), and Radial Velocity Scatter Information (RV$_{SCATTER}$)

APOGEE-2 ID	[M/H] (dex)	$J_{2MASS} - K_{s,2MASS}$ (mag)	E(B-V)	T_{eff}^{pho} (K)	$\log^{iso}$ (dex)	$Teff_{ASPCAP}^{a}$ (K)	$\log g_{ASPCAP}^{a}$ (dex)	N_{visits}	S/N (pixel^{-1})	RV (km s^{-1})	RV$_{SCATTER}$ (km s^{-1})	$\langle r_{peri}\rangle$ (kpc)	$\langle r_{apo}\rangle$ (kpc)	$\langle Z_{max}\rangle$ (kpc)	$\langle e\rangle$	Orbit
2M13314691 +2804210[a]	−1.08	0.907	0.009	4048.1	0.646	4114.6	1.381	4	248	−1.72	0.12	$0.49^{0.56}_{0.22}$	$10.25^{10.70}_{9.89}$	$6.33^{7.53}_{6.15}$	$0.91^{0.96}_{0.89}$	Retrograde
2M15153684 +3501283	−0.99	0.77	0.017	4401.3	1.341	4379.2	1.808	3	115	−308.45	0.12	$1.84^{1.88}_{1.78}$	$20.13^{25.59}_{17.75}$	$15.81^{23.85}_{13.55}$	$0.84^{0.86}_{0.81}$	Retrograde
2M16092248 +2449223[a]	−1.14	0.971	0.070	3990.5	0.539	4095.6	1.237	5	364	−92.30	0.22	$0.11^{0.96}_{0.05}$	$9.01^{9.25}_{8.45}$	$6.24^{7.62}_{5.39}$	$0.98^{0.99}_{0.81}$	Retrograde
2M16300791 +2537503	−1.09	0.67	0.035	4717.5	1.851	4785.8	2.169	2	143	−255.29	0.02	$0.61^{0.65}_{0.53}$	$7.65^{7.72}_{7.46}$	$6.81^{6.92}_{6.78}$	$0.85^{0.87}_{0.84}$	Retrograde
2M16482145 −1930487	−0.96	1.013	0.520	4638.1	1.767	4377.4	1.741	3	97	65.98	0.01	$0.15^{0.35}_{0.02}$	$4.96^{5.48}_{4.29}$	$2.64^{3.39}_{2.29}$	$0.93^{0.99}_{0.88}$	Prograde
2M17155274 +2907368	−1.07	0.839	0.058	4287.6	1.076	4313.9	1.601	2	94	−81.42	0.00	$0.76^{0.82}_{0.65}$	$9.19^{9.68}_{8.93}$	$6.98^{8.63}_{6.05}$	$0.85^{0.87}_{0.83}$	Prograde
2M17214096 +4246147	−1.11	0.777	0.020	4385.1	1.249	4439.0	1.614	5	181	−298.07	0.05	$1.43^{1.46}_{1.42}$	$9.34^{10.16}_{9.06}$	$4.03^{4.48}_{3.84}$	$0.73^{0.75}_{0.72}$	Retrograde
2M17502038 −2805411	−1.09	3.492	...	...	...	3775.0	0.487	2	101	−53.06	0.13	...	...	...	...	...
2M18070782 −1517393[a]	−1.07	1.66	...	...	...	3924.7	1.126	3	151	−370.42	0.02	...	...	...	...	...
2M19281906 +4915086	−1.22	0.79	0.086	4460.6	1.303	4309.0	1.715	3	422	−302.89	0.18	...	...	...	...	...
2M23341347 +4836321	−1.17	1.027	0.196	4048.9	0.566	4073.1	1.227	3	205	−168.33	0.15	$0.29^{0.54}_{0.11}$	$17.76^{20.21}_{17.29}$	$3.20^{4.69}_{2.98}$	$0.97^{0.99}_{0.94}$	Prograde

	[Fe/H]sp	[C/Fe]sp	[N/Fe]sp	[O/Fe]sp	[Mg/Fe]sp	[Al/Fe]sp	[Si/Fe]sp	[Ce/Fe]sp	[Nd/Fe]sp
2M13314691 +2804210	−1.07	0.02	0.26	0.43	0.38	0.88	0.85	0.73	...
2M15153684 +3501283	−0.99	0.12	0.25	0.43	0.29	0.78	0.81	0.65	...
2M16092248 +2449223	−1.11	−0.17	0.38	0.43	0.40	0.86	0.99	0.72	0.77
2M16300791 +2537503	−1.04	0.01	0.41	0.50	0.34	0.94	0.78	0.33	...
2M16482145 −1930487	−0.99	0.12	0.39	0.50	0.32	0.81	0.81	...	0.89
2M17155274 +2907368	−1.07	0.01	0.20	0.41	0.43	...	0.73	0.30	...
2M17214096 +4246147	−1.08	−0.16	0.40	0.44	0.46	0.97	1.06	0.76	...
2M17502038 −2805411	−1.09	−0.14	0.35	0.42	0.42	...	0.80	0.45	...
2M18070782 −1517393	−0.98	0.10	0.15	0.33	0.39	0.70	0.67	0.70	...
2M19281906 +4915086	−1.20	−0.21	0.41	0.36	0.20	0.74	0.76	...	...
2M23341347 +4836321	−1.14	−0.04	0.30	0.40	0.39	0.85	0.80	0.70	...

Table 2
(Continued)

	[Fe/H]pho	[C/Fe]pho	[N/Fe]pho	[O/Fe]pho	[Mg/Fe]pho	[Al/Fe]pho	[Si/Fe]pho	[Ce/Fe]pho	[Nd/Fe]pho
2M13314691 +2804210	−1.23	−0.09	0.44	0.44	0.37	0.77	0.79	0.41	...
2M15153684 +3501283	−1.00	−0.01	0.36	0.50	0.51	0.88	0.78	0.38	...
2M16092248 +2449223	−1.26	−0.26	0.52	0.35	0.29	0.62	0.81	0.41	0.41
2M16300791 +2537503	−1.09	−0.04	0.48	0.48	0.38	0.93	0.83	0.39	...
2M16482145 −1930487	−0.89	0.06	0.59	0.81	0.44	0.94	0.69	...	0.81
2M17155274 +2907368	−1.14	−0.08	0.33	0.44	0.58	...	0.69	0.32	...
2M17214096 +4246147	−1.13	−0.24	0.48	0.42	0.53	0.99	1.05	0.52	...
2M17502038 −2805411	...	...	...	...	...	...	...	...	...
2M18070782 −1517393	...	...	...	...	...	...	...	...	...
2M19281906 +4915086	−1.16	−0.28	0.51	0.63	0.38	0.90	0.67	...	...
2M23341347 +4836321	−1.22	−0.17	0.47	0.44	0.53	0.92	0.78	0.36	...

Note. The average value of the orbital elements (pericentric and apocentric radii, the maximum distance the orbit reaches above/below the Galactic plane, and the eccentricity) were found for one million realizations, with uncertainty ranges given by the 16th (subscript) and 84th (superscript) percentile values. Rows 14–37: mean elemental abundances derived of our target stars using the "abund" module in BACCHUS code, adopting the atmospheric parameters from ASPCAP/APOGEE-2 (abundances labeled as [Fe/H]sp and [X/Fe]sp) and atmospheric parameters from photometry and isochrones (abundances labeled as [Fe/H]pho and [X/Fe]pho). The solar reference abundances are from (Asplund2005). The BACCHUS pipeline was used to derive the broadening parameters, metallicity, and chemical abundances.

[a] Uncalibrated ASPCAP parameters are listed in columns 7 and 8.
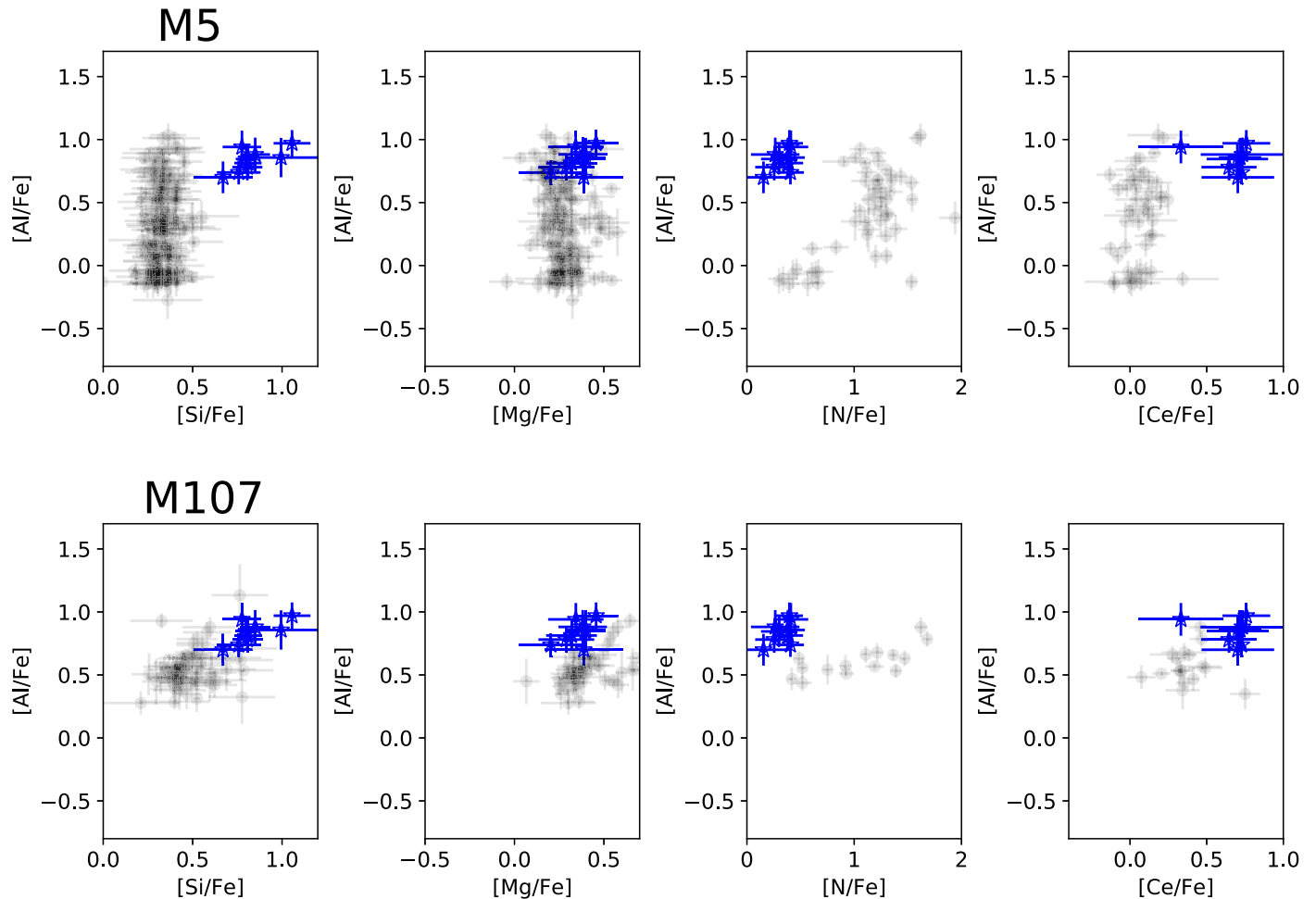
Figure 5. M5 and M107 cluster stars from Masseron et al. (2019) are shown as filled gray dots in the Si–Al, Mg–Al, N–Al, and Ce–Al planes. The crosses indicate typical error bars. The Si–Al-rich stars are indicated with blue star symbols.

modest enrichment in magnesium. In fact, most of the stars in our sample replicate (or exceed) the extreme abundance patterns of Galactic GCs, highlighting the uniqueness of these environments, as seen in Figure 5. That is because it is very likely that silicon-rich stars are proposed to have been gestated in similar molecular clouds as Galactic GCs, thus sharing their environmental origin. However, it is less obvious in the [N/Fe]–[Al/Fe] plane, where the bulk of stars in Galactic GC environments follow a clear correlation between [N/Fe] and [Al/Fe] (depending on the cluster or data set), that this plot indicates that the GC stars follow a slightly different N–Al enrichment that runs parallel to those observed in the silicon-rich stars. It is important to note that silicon-rich stars were indeed discovered in GCs and in the inner stellar halo of the Milky Way (this study), but it is noteworthy that none so far have been identified in the disk of the galaxy.

3.3. Polluter Candidates

The origin of silicon-rich stars can be ascribed to different processes. If we allow a brief venture into the realm of speculation, it could be possible that mildly metal-poor giant stars with Si overabundances could also originate through gas already strongly enriched from massive supernovae (SNe; $M > 20\,M_{\odot}$), pair-instability SNe (PISNe), hypernovae (with stellar progenitor masses greater than $>140\,M_{\odot}$), and/or faint SNe (see Nomoto et al. 2013); however, many of these events involve the total destruction of the star, with no remnant left behind (Kemp et al. 2018). Thus, the anomalously high levels of [Si/Fe] may be a result of the huge masses of processed material released from explosive nucleosynthesis of core-collapse SNe (SNe II) events, which can explain the abundance feature of the silicon-rich giants. However, with the limited chemical species available in this study a single source of pollution is probably not enough to fit all the multi-element observations. More stringent conclusions will be drawn when the full set of light/heavy elements is available.

Finally, combining the absence of radial velocity variation (RV$_{\rm SCATTER} < 0.5\,{\rm km\,s^{-1}}$, as listed in Table 2) and silicon overabundance does not provide enough information to support any hypothesis of such objects possibly being formed in a binary system.

Conversely, the population of silicon-rich GC stars has been understood by invoking an internal production of Si, which is likely due to the increased leakage from the Mg–Al cycle on ^{28}Si, i.e., when the ^{27}Al(p, γ)^{28}Si reaction takes over ^{27}Al(p, α)^{24}Mg, a certain amount of ^{28}Si is thus produced by proton-captures (Karakas & Lattanzio 2003). This overproduction of Si typically occurs at temperatures >100 MK (Arnould et al. 1999), in a similar way to that recently detected in GC stars (Carretta & Bragaglia 2019; Masseron et al. 2019). The fact that the leakage from Mg–Al cycle on ^{28}Si is apparently confined to GC environments implies that the process

responsible for field stars with enhanced silicon may be tied to a certain epoch in the Milky Way's evolution similar to GC stars at a similar metallicity.

4. Concluding Remarks

In conclusion, we find evidence of a unique collection of 11 mildly metal-poor giant stars that display unexpected and anomalously high levels of [Si/Fe] ($>+0.6$, which we henceforth refer to as silicon-rich stars), peaking at [Fe/H] ~ -1.07. In principle, this new subpopulation forms a distinct track in the abundance plane, different from the Milky Way's field stars, supporting the identification of a separate origin. Here, we speculate that such stars could be former member GCs that still exist, or ancient clusters that were tidally disrupted. Whether these objects are mostly some of the oldest stars in the Milky Way is still yet to be determined.

Furthermore, our dynamical study indicates that most of the silicon-rich stars selected so far possess halo-like and retrograde orbits passing through the bulge and disk of the Milky Way, which suggests that silicon-rich stars among field stars are either good candidates to be escaped GC stars and/or the debris clues of GCs born in dwarf galaxies accreted to the Milky Way that eventually got dissolved, spraying their stars across the Milky Way halo (Zinn 1993; Majewski et al. 2012; Kruijssen et al. 2019). We speculate that this new stellar subpopulation we discovered in the inner stellar halo may thus be the tracer of a global phenomenon where these stars were necessarily formed in Galactic GCs and were later lost to the field, such as ω Centauri (Ibata et al. 2019). However, a future inventory of the chemistry of these objects, in particular, the elements formed by neutron-capture processes, would hint at their origin, and possibly help confirm or refute the association with Galactic GC stars.

ORCID iDs

Timothy C. Beers ⓘ https://orcid.org/0000-0003-4573-6233
Vinicius M. Placco ⓘ https://orcid.org/0000-0003-4479-1265
Edmundo Moreno ⓘ https://orcid.org/0000-0001-6450-2315
Dante Minniti ⓘ https://orcid.org/0000-0002-7064-099X
Baitian Tang ⓘ https://orcid.org/0000-0002-0066-0346
Angeles Pérez-Villegas ⓘ https://orcid.org/0000-0002-5974-3998
Sandro Villanova ⓘ https://orcid.org/0000-0001-6205-1493

References

Abolfathi, B., Aguado, D. S., Aguilar, G., et al. 2018, ApJS, 235, 42
Anders, F., Khalatyan, A., Chiappini, C., et al. 2019, A&A, 628, A94
Arnould, M., Goriely, S., & Jorissen, A. 1999, A&A, 347, 572
Barbuy, B., Chiappini, C., & Gerhard, O. 2018, ARA&A, 56, 223

Bovy, J., Leung, H. W., Hunt, J. A. S., et al. 2019, MNRAS, 490, 4740
Carollo, D., Beers, T. C., Chiba, M., et al. 2010, ApJ, 712, 692
Carretta, E., & Bragaglia, A. 2019, A&A, 627, L7
Fernández-Trincado, J. G., Beers, T. C., Tang, B., et al. 2019a, MNRAS, 488, 2864
Fernández-Trincado, J. G., Mennickent, R., Cabezas, M., et al. 2019b, A&A, 631, A97
Fernández-Trincado, J. G., Moreno, E., & Pérez-Villegas, A. 2019c, arXiv:1904.05370
Fernández-Trincado, J. G., Robin, A. C., Moreno, E., et al. 2016, ApJ, 833, 132
Fernández-Trincado, J. G., Zamora, O., García-Hernández, D. A., et al. 2017, ApJL, 846, L2
García Pérez, A. E., Allende Prieto, C., Holtzman, J. A., et al. 2016, AJ, 151, 144
Hasselquist, S., Carlin, J. L., Holtzman, J. A., et al. 2019, ApJ, 872, 58
Hawkins, K., Jofré, P., Masseron, T., & Gilmore, G. 2015, MNRAS, 453, 758
Hayes, C. R., Majewski, S. R., Shetrone, M., et al. 2018, ApJ, 852, 49
Ibata, R. A., Bellazzini, M., Malhan, K., Martin, N., & Bianchini, P. 2019, NatAs, 3, 667
Karakas, A. I., & Lattanzio, J. C. 2003, PASA, 20, 279

Kemp, A. J., Casey, A. R., Miles, M. T., et al. 2018, MNRAS, 480, 1384
Koch, A., Grebel, E. K., & Martell, S. L. 2019, A&A, 625, A75
Kruijssen, J. M. D., Pfeffer, J. L., Reina-Campos, M., Crain, R. A., & Bastian, N. 2019, MNRAS, 486, 3180
Lindegren, L., Hernández, J., Bombrun, A., et al. 2018, A&A, 616, A2
Lucatello, S., Beers, T. C., Christlieb, N., et al. 2006, ApJL, 652, L37
Majewski, S. R., Nidever, D. L., Smith, V. V., et al. 2012, ApJL, 747, L37
Majewski, S. R., Schiavon, R. P., Frinchaboy, P. M., et al. 2017, AJ, 154, 94
Martell, S. L., Shetrone, M. D., Lucatello, S., et al. 2016, ApJ, 825, 146
Masseron, T., García-Hernández, D. A., Mészáros, S., et al. 2019, A&A, 622, A191
Masseron, T., Merle, T., & Hawkins, K. 2016, BACCHUS: Brussels Automatic Code for Characterizing High accUracy Spectra, Astrophysics Source Code Library, ascl:1605.004
Nidever, D. L., Holtzman, J. A., Allende Prieto, C., et al. 2015, AJ, 150, 173
Nomoto, K., Kobayashi, C., & Tominaga, N. 2013, ARA&A, 51, 457
Pereira, C. B., Holanda, N., Drake, N. A., & Roig, F. 2019, AJ, 157, 70
Queiroz, A. B. A., Anders, F., Santiago, B. X., et al. 2018, MNRAS, 476, 2556
Schiavon, R. P., Zamora, O., Carrera, R., et al. 2017, MNRAS, 465, 501
Zinn, R. 1993, in ASP Conf. Ser. 48, The Globular Cluster-Galaxy Connection, ed. G. H. Smith & J. P. Brodie (San Francisco, CA: ASP), 302